Biophysical Journal, Volume *113*

Supplemental Information

Mechanisms Responsible for ω-Pore Currents in Ca_v Calcium Channel Voltage-Sensing Domains

Stefania Monteleone, Andreas Lieb, Alexandra Pinggera, Giulia Negro, Julian E. Fuchs, Florian Hofer, Jörg Striessnig, Petronel Tuluc, and Klaus R. Liedl

Supplemental Information - Figures

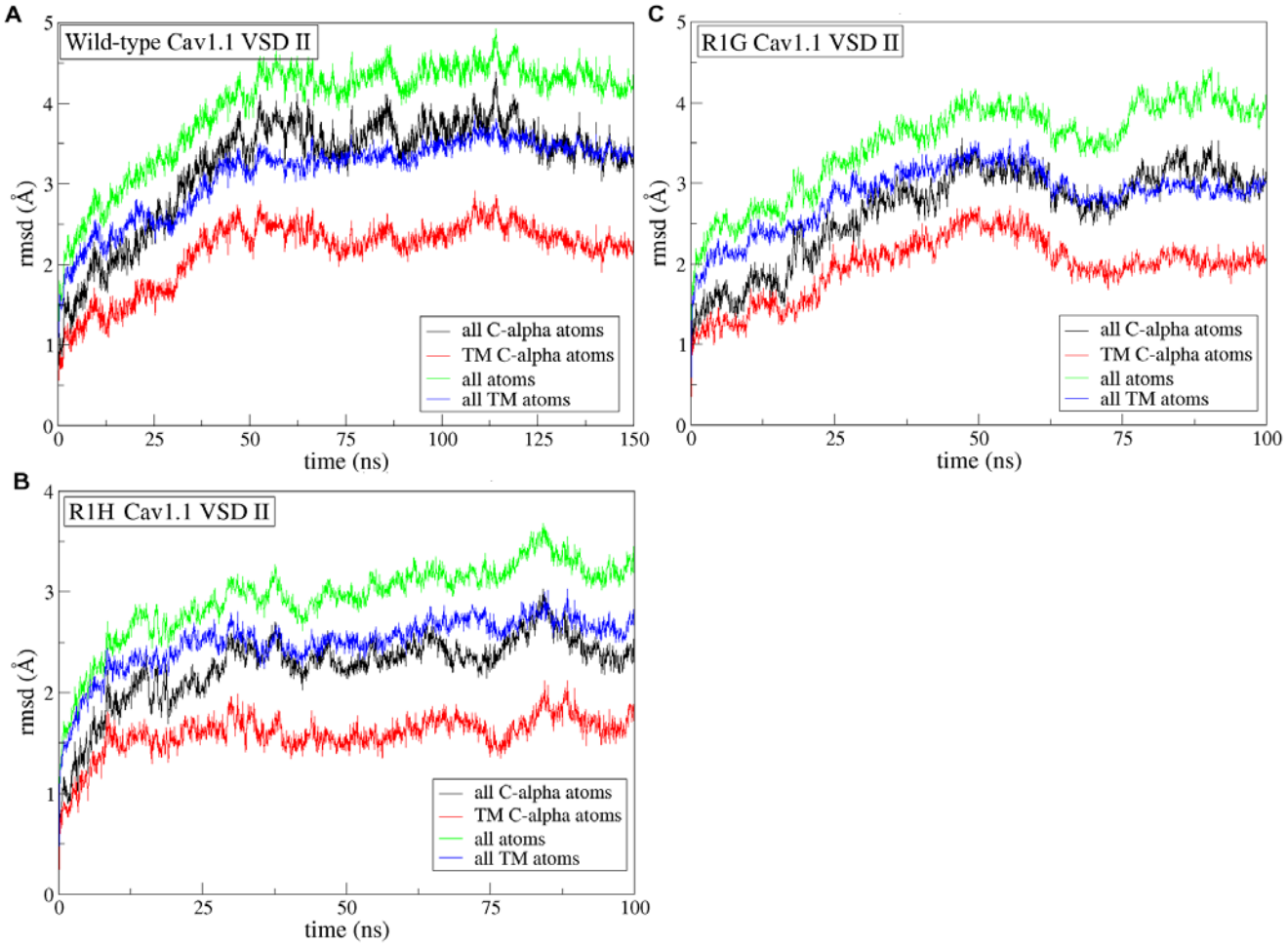

Figure 1: *Root mean square deviation of wild-type (A), R1H (B) and R1G (C) mutant VSD of $Ca_v1.1$ domain II in the resting state α.*

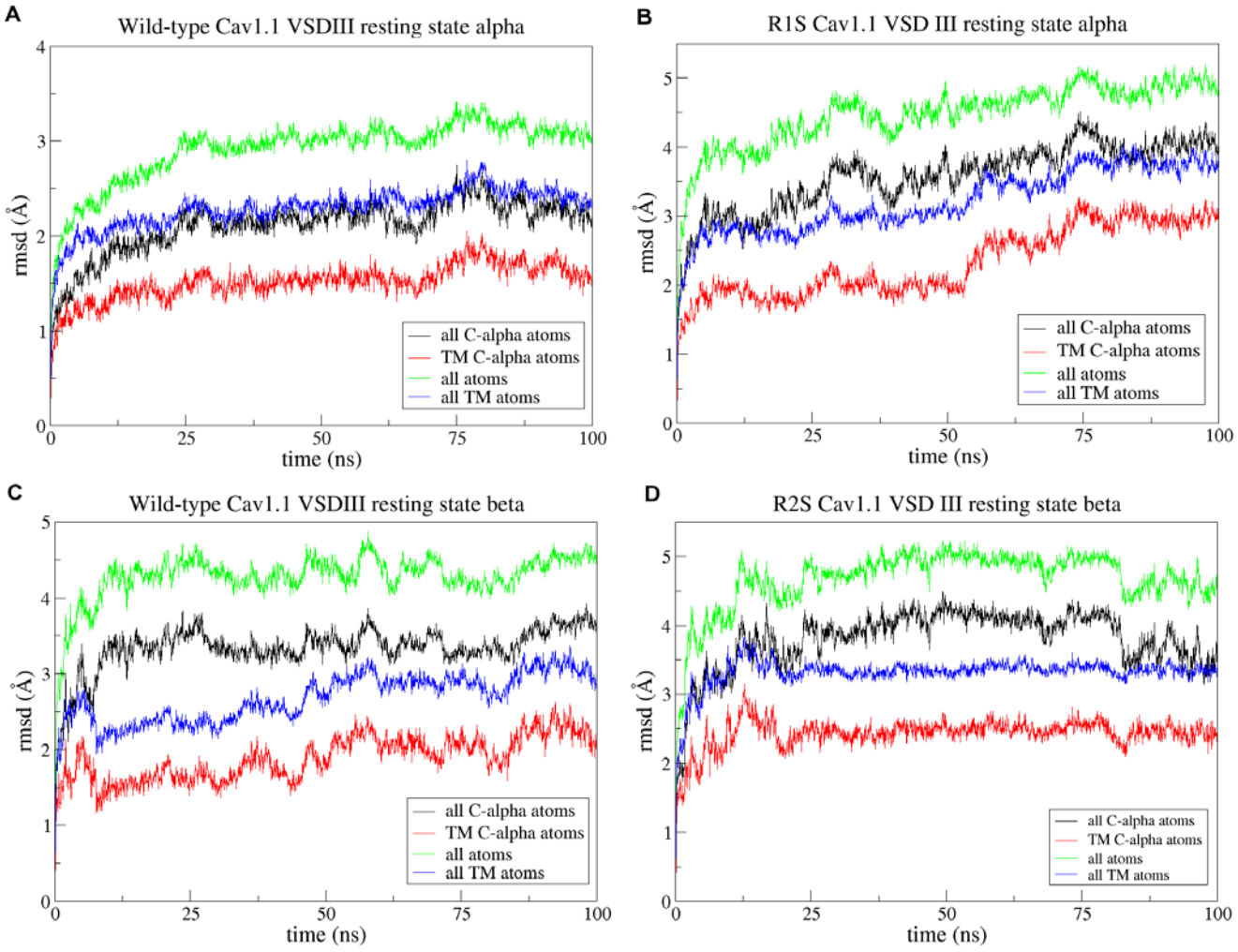

Figure 2: *Root mean square deviation of wild-type, R1S and R2S mutant VSD of $Ca_v1.1$ domain III in the resting state α and β.*

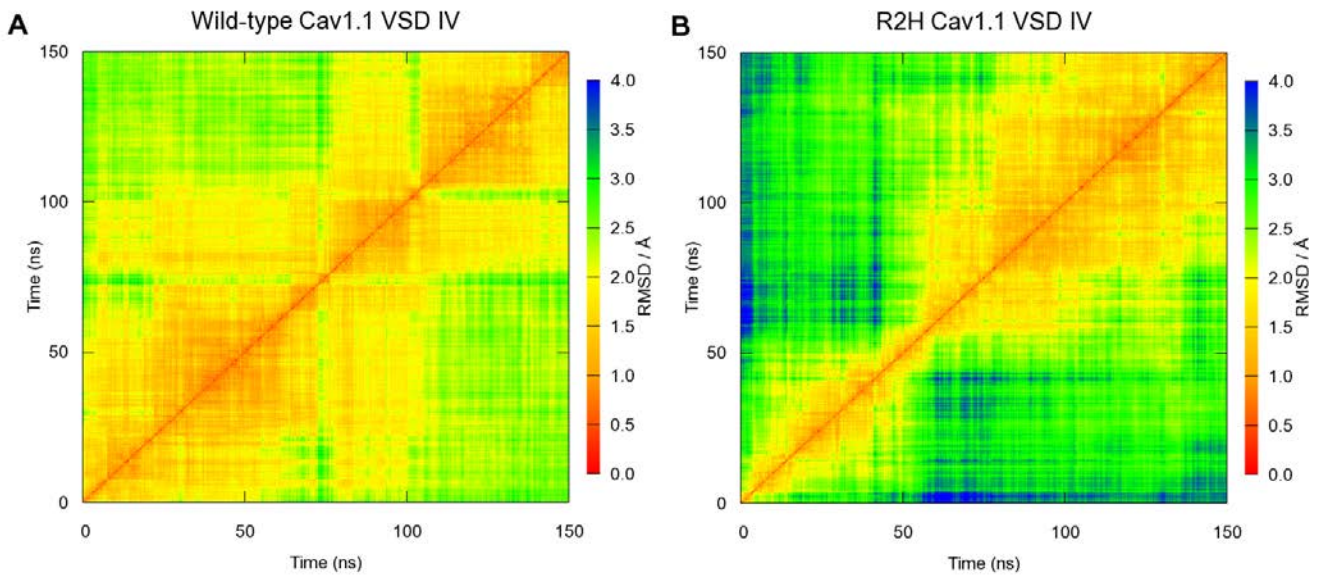

Figure 3: *2d-rmsd of all Cα atoms in wild-type (A) and R2H mutant (B) VSD of $Ca_v1.1$ domain IV in the resting state β. The wild-type protein is more stable than the mutant as the simulation converges earlier. Whereas the MD simulation of the mutant requires a longer simulation time to converge.*

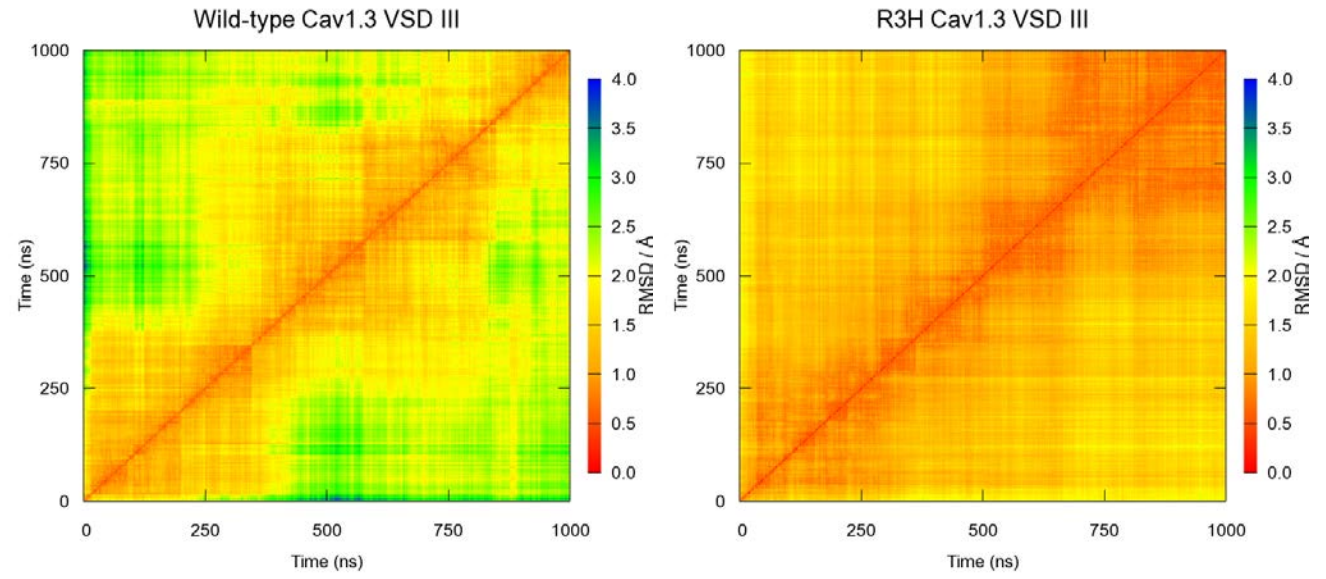

Figure 4: *2d-rmsd of transmembrane Cα atoms in wild-type (A) and R3H mutant (B) VSD of $Ca_v1.3$ domain III in the resting state β.*

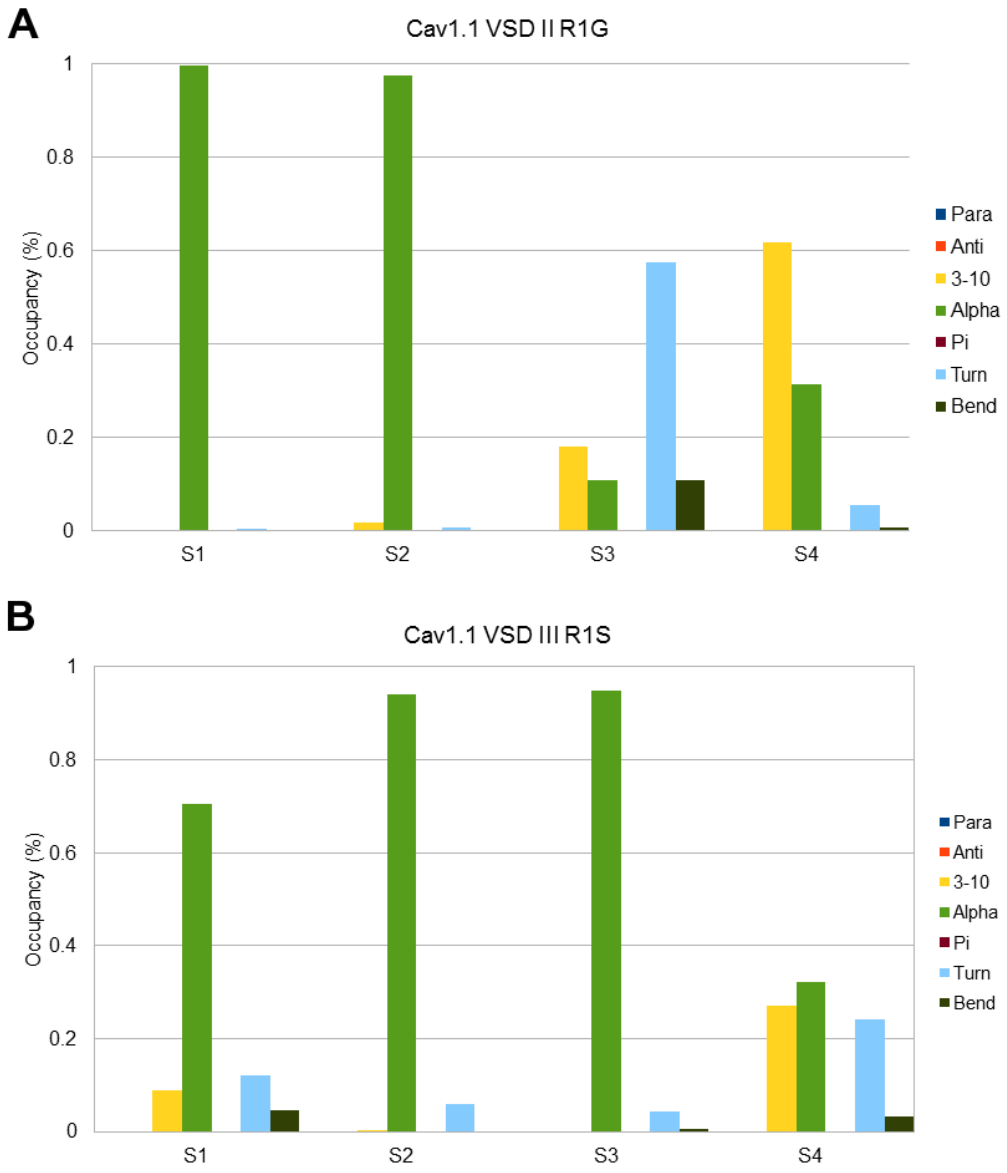

Figure 5: *Averaged occupancy values over 100 ns and whole transmembrane segments in the resting state α of the $Ca_v1.1$ VSD of domain II R1G (**A**) and III R1S (**B**).*

A: *Compared to the wild-type, segment S3 loses its helical secondary structure and changes toward a beta turn.*

B: *All segments show a prevalent alpha helical secondary structure, but S4 presents also 3-10 helix and beta turn patterns.*

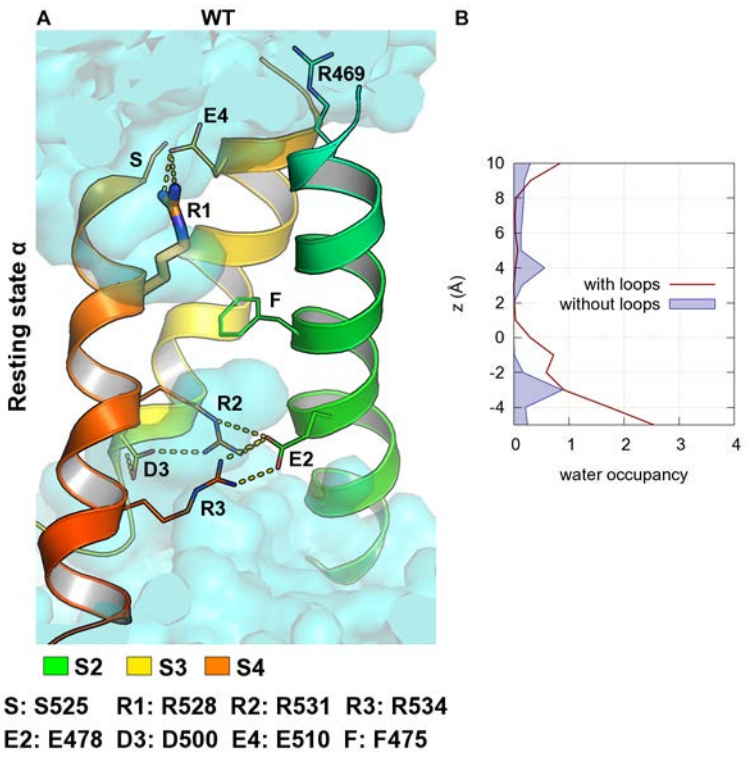

Figure 6*. (**A**) WT II domain VSD in the resting state α modelled without intra- and extra-cellular linkers. The only difference to the model including loops (Fig. 1) is that R1 forms ionic interactions with E4 because E452 from S1-S2 loop was removed from the structure. (**B**) The presence or absence of loops does not affect the water occupancy in the center of the VSD.*

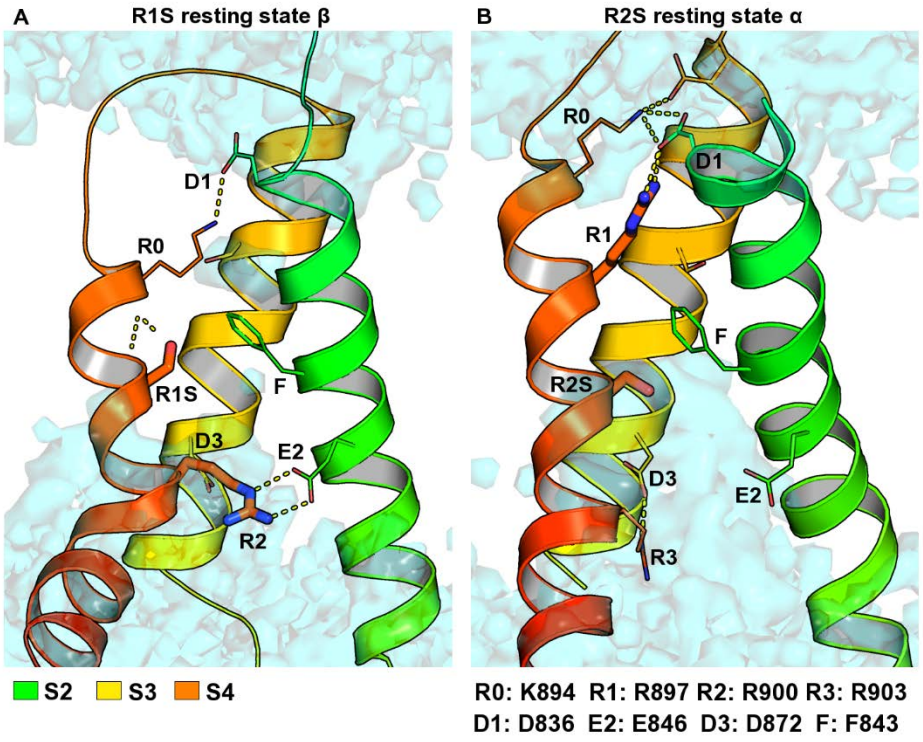

Figure 7: *R1S and R2S mutant VSDs of domain III in the resting state β (**A**) and α (**B**). The protein is represented as cartoons, colored as rainbow according to the residue number: segment S1, lipids and hydrogen atoms are not shown for clearness. Gating charges are shown as lines, whereas mutated residues are highlighted as sticks. H-bonds are marked with yellow dots. Average water density during the simulation is shown as transparent cyan surface. The average number of water molecules in the VSD is calculated for each frame.*

A: *R1S does not result in a water wire in the resting state β because R0 and R2 seal the center of the VSD. R1S forms H-bond interactions with the backbone of S4 that are conserved in helical secondary structure elements. The ionic interaction between R2 and E2 causes a conformational change of helix S4 that forms a kink at R2 level.*

B: *in the resting state α, R2S does not cause a water wire as water molecules can enter only from the cytoplasm. R2S is close to F and loses the ionic interaction with the counter charges in S2 and S3.*

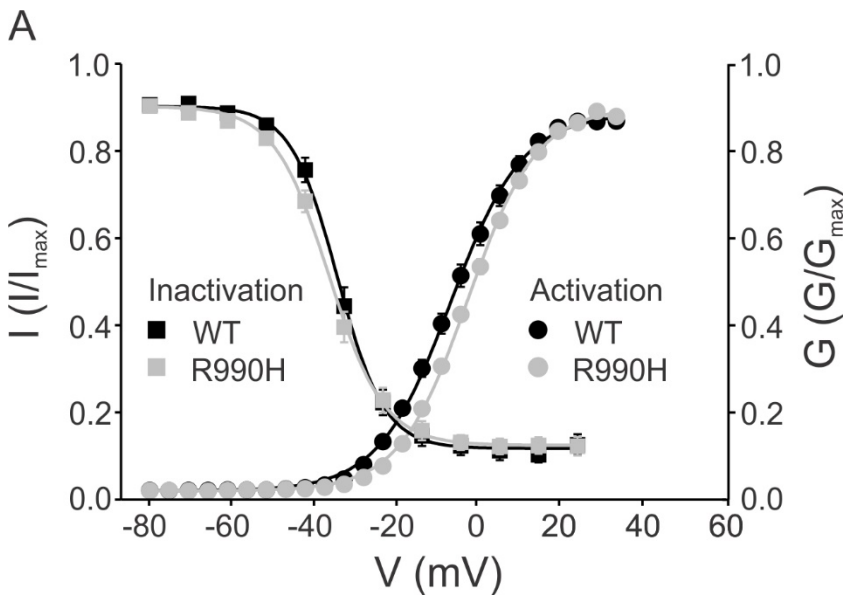

Figure 8: Mutation of R1 charge to His in $Ca_V1.3$ channel does not alter the voltage dependence of the steady-state inactivation. *A. Voltage dependence of steady state inactivation (squares) was measured by applying a control test pulse (20 ms to the voltage of maximal inward current, V_{max}) followed by 5-s conditioning steps to various potentials and a subsequent 20-ms test pulse to V_{max} (30-s recovery between sweeps). Inactivation was calculated as the ratio between the current amplitudes of the test versus control pulse. Whereas the voltage-dependence of activation (circles) of $Ca_V1.3$-R990H was significantly shifted by ~3 mV towards more depolarizing potentials compared to WT $Ca_V1.3$ channel (same data as in Figure 5B), the voltage dependence of steady-state inactivation (WT $V_{0.5}$ =-30.8 ± 1.14, n=16; R990H $V_{0.5}$ = -32.5 ± 1.12, n = 18) or the slope of the voltage dependence of inactivation (WT k=5.38 ±0.30, n=16; R990H k = 6.76 ± 0.39, n=18) were not altered.*

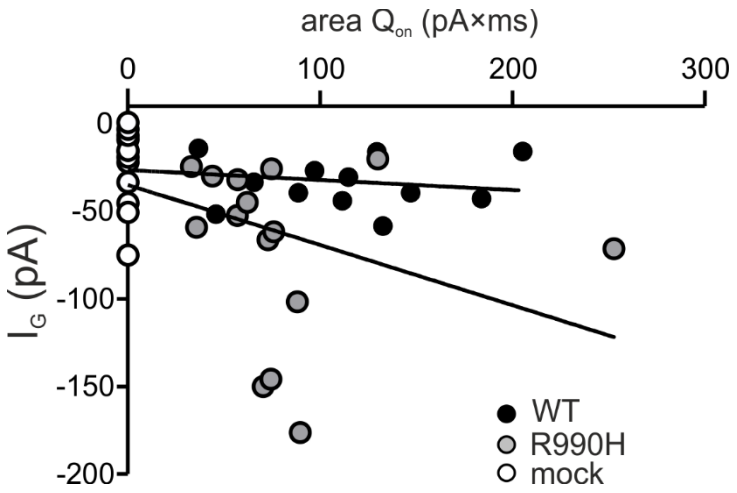

Figure 9. The amplitude of $Ca_V1.3$-R990H guanidinium current (I_G) negatively correlates with the number of channels functionally incorporated in the membrane (Q_{ON}). *The linear regression fit of the dependence between I_G measured at -100 mV and the Q_{ON} measured at the reversal potential shows a statistically significant correlation for the $Ca_V1.3$-R990H ($p < 0.05$) but not for WT $Ca_V1.3$. Since our experimental data shows that the mock transfected cells (no α_1 subunit) (N=12) also conduct a guanidinium current we included these values in both WT (N=12) and R990H (N=15) fit functions. Statistics calculated using One Way Repeated Measurements ANOVA with Bonferroni t-test.*

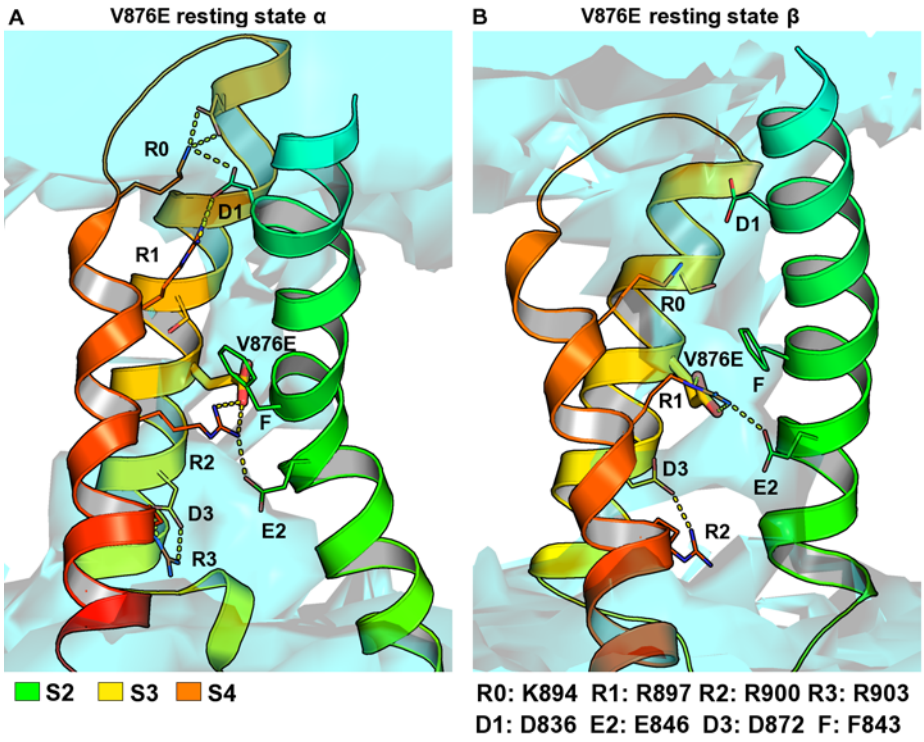

Figure 10. $Ca_V1.1$ III VSD bearing the V876E mutation modelled in the resting state α (A) and β (B). *The modelling predicts the formation of a water wire independent of the gating state. In the resting state α, V876E forms ionic interactions with R2, which moves upwards compared to WT and allows E2 to interact with water molecules. In addition, V876E drives water to the hydrophobic center, which becomes polar due to the introduction of a charged amino acid. In the resting state β, the ionic interactions of R2 with V876E are replaced by R1.*

Supplemental Information - Tables

Table 1: *Up-to-date list of mutations in voltage-gated calcium channels that develop or might develop omega currents. Highlighted cells indicate experimentally measured omega-currents. For further mutations at voltage sensors of ion channels we refer to the review of Jurkat-Rott et al. (1).*

Isoform	Domain	Mutation	N.	Disease	References	Functional Effect
Cav1.1	I	R174W	R4	MHS	(2)	α-pore gain of function
	II	R528G/H	R1	HPP	(3-9)	α-pore gain or loss of function and ω-current
		R528C	R1	HPP	(10)	n.c.
	III	V876E		HPP		n.c.
		R897S	R1	HPP	(11)	n.c.
		R900G/S	R2	HPP	(12, 13)	n.c.
	IV	R1239G/H	R2	HPP	(7-9, 14, 15)	α-pore gain of function and leak current
Cav1.3	II	R619W	R1	APAs	(16)	n.c.
	III	R990H	R3	APAs	(17)	α-pore not affected but ω-current
Cav2.1	I	R192Q	R0	FHM	(18-21)	α-pore gain of function
		R195K	R1	FHM	(22)	n.c.
	II	R583Q	R1	FHM	(22-24)	α-pore gain of function
	III	R1347Q	R1	FHM	(25, 26)	n.c.
		R1350Q	R2	EA2	(27, 28)	α-pore gain of function
	IV	R1661H	R1	FHM	(29)	n.c.
		R1664Q	R2	FHM	(30)	n.c.
		R1667W	R3	FHM	(22)	n.c.

APAs: adrenal aldosterone-producing adenomas
EA2: episodic ataxia type 2
FHM: familial hemiplegic migraine
HPP: hypokalemic periodic paralysis
MHS: malignant hyperthermia susceptibility

Table 2: Sequence alignment of $Ca_v1.1$, $Ca_v1.3$ and $Ca_v2.1$ voltage sensors. *Green highlighted residues represent the gating charges R1 to R4; yellow highlighted residues indicate other positively charged positions of segment S4. Residues for which mutants have been identified are highlighted in red.*

		R0	X	X	R1	X	X	R2	X	X	R3	X	X	R4	X	X	R5	X	X	R6
Cav1.1	I	K	A	L	R	A	F	R	V	L	R	P	L	R	L	V	S	G	V	P
	II	S	V	L	R	C	I	R	L	L	R	L	F	K	I	T	K	Y	W	T
	III	K	I	L	R	V	L	R	V	L	R	P	L	R	A	I	N	R	A	K
	IV	A	F	F	R	L	F	R	V	M	R	L	V	K	L	L	N	R	A	E
Cav1.3	I	K	A	L	R	A	F	R	V	L	R	P	L	R	L	V	S	G	V	P
	II	S	V	F	R	C	V	R	L	L	R	L	F	K	V	T	R	H	W	T
	III	K	I	L	R	V	L	R	V	L	R	P	L	R	A	I	N	R	A	K
	IV	T	F	F	R	L	F	R	V	M	R	L	V	K	L	L	S	R	G	E
Cav2.1	I	R	T	L	R	A	V	R	V	L	R	P	L	K	L	V	S	G	I	P
	II	S	V	L	R	A	L	R	L	L	R	I	F	K	V	T	K	Y	W	A
	III	K	S	L	R	V	L	R	V	L	R	P	L	K	T	I	K	R	L	P
	IV	S	F	L	R	L	F	R	A	A	R	L	I	K	L	L	R	Q	G	Y

Table 3: Gating charges and counter charges in voltage sensors of $Ca_v1.1$ domains II, III and IV and $Ca_v1.3$ domain III.

	Cav1.1			Cav1.3
	VSD II	VSD III	VSD IV	VSD III
F	F475	F843	F1161	F930
R0	S525, R469	K894	R1229	K981
R1	R528	R897	R1236	R984
E1/D1	E452	D836	-	D923
R2	R531	R900	R1239	R987
E2	E478	E846	E1164	E933
R3	R534	R903	R1242	R990
D3	D500	D872	D1186	D959
E4/D4	E510	-	D1196	-

Table 4: Ionic interactions between gating and counter charges in WT voltage sensors at distinct resting states.

Gating charge	Counter charge				
	Cav1.1				Cav1.3
	II	III		IV	III
	State α	State α	State β	State β	State β
R0	E4	D1	D1	D4	-
R1	E452	D1	E2	D4	D1
R2	E2	E2, D3	D3	E2, D3	D3
R3	E2	D3	-	D3	E2

Table 5: Averaged helical secondary structure occupancy over 100 ns of whole transmembrane segments for WT and mutant VSDs in distinct states.

System			State	S1	S2	S3	S4
$Ca_v1.1$	Domain II	WT	Resting α	98%	99%	56%	67%
		R1H		98%	99%	58%	77%
		R1G		100%	99%	**29%**	93%
	Domain III	WT	Resting α	89%	92%	85%	76%
			Resting β	96%	85%	94%	93%
		R1S	Resting α	79%	94%	95%	**59%**
			Resting β	99%	98%	89%	83%
		R2S	Resting α	92%	95%	99%	89%
			Resting β	80%	76%	95%	**66%**
	Domain IV	WT	Resting β	88%	98%	95%	67%
		R2H		99%	97%	97%	85%
$Ca_v1.3$	Domain III	WT	Resting β	83%	91%	82%	75%
		R3H		86%	93%	78%	75%

Table 6: H-bond counts for WT and R2S mutant of $Ca_v1.1$ domain III in distinct states. *Gating charges are positively charged amino acids in the transmembrane segment S4. Counter charges are negatively charged residues in the surrounding segments in the voltage sensor.*

In the WT VSD, R2 forms H-bonds with counter charges (E2 and D3), polar amino acids and water molecules. In the mutant, R2S loses the interactions with counter charges in the resting state α whereas in the resting state β it can still form H-bonds with a negatively charged residue in the helix S3 (D3).

	Resting state α		**Resting state β**	
	WT	**R2S**	**WT**	**R2S**
Gating charges	0	72%	0	1%
Counter charges	100%	0	97%	85%
Polar residues	0	1%	67%	0
Water	93%	7%	23%	0

Table 7: H-bond counts for WT and R3H mutant of $Ca_v1.3$ domain III in distinct states.

In the WT voltage sensor, R3 forms H-bonds with counter charges and water molecules. In the mutant, R3H loses the interactions with counter charges, but forms H-bonds with polar residues in the active state and water molecules in the resting state β.

	Active state		**Resting state β**	
	WT	**R3H**	**WT**	**R3H**
Gating charges	0	0	0	17%
Counter charges	33%	0	80%	1%
Polar residues	0	84%	0	8%
Water	55%	0	20%	67%

References

1. Jurkat-Rott, K., J. Groome, and F. Lehmann-Horn. 2012. Pathophysiological role of omega pore current in channelopathies. Front Pharmacol 3:112.
2. Striessnig, J., H. J. Bolz, and A. Koschak. 2010. Channelopathies in Cav1.1, Cav1.3, and Cav1.4 voltage-gated L-type Ca2+ channels. Pflugers Arch 460:361-374.
3. Jurkat-Rott, K., F. Lehmann-Horn, A. Elbaz, R. Heine, R. G. Gregg, K. Hogan, P. A. Powers, P. Lapie, J. E. Vale-Santos, J. Weissenbach, and et al. 1994. A calcium channel mutation causing hypokalemic periodic paralysis. Hum Mol Genet 3:1415-1419.
4. Lapie, P., C. Goudet, J. Nargeot, B. Fontaine, and P. Lory. 1996. Electrophysiological properties of the hypokalaemic periodic paralysis mutation (R528H) of the skeletal muscle alpha 1s subunit as expressed in mouse L cells. FEBS Lett 382:244-248.
5. Jurkat-Rott, K., U. Uetz, U. Pika-Hartlaub, J. Powell, B. Fontaine, W. Melzer, and F. Lehmann-Horn. 1998. Calcium currents and transients of native and heterologously expressed mutant skeletal muscle DHP receptor α1 subunits (R528H). FEBS Letters 423:198-204.
6. Morrill, J. A., R. H. Brown, Jr., and S. C. Cannon. 1998. Gating of the L-type Ca channel in human skeletal myotubes: an activation defect caused by the hypokalemic periodic paralysis mutation R528H. J Neurosci 18:10320-10334.
7. Morrill, J. A., and S. C. Cannon. 1999. Effects of mutations causing hypokalaemic periodic paralysis on the skeletal muscle L-type Ca2+ channel expressed in Xenopus laevis oocytes. J Physiol 520 Pt 2:321-336.
8. Kuzmenkin, A., C. Hang, E. Kuzmenkina, and K. Jurkat-Rott. 2007. Gating of the HypoPP-1 mutations: I. Mutant-specific effects and cooperativity. Pflugers Arch 454:495-505.
9. Jurkat-Rott, K., M.-A. Weber, M. Fauler, X.-H. Guo, B. D. Holzherr, A. Paczulla, N. Nordsborg, W. Joechle, and F. Lehmann-Horn. 2009. K+-dependent paradoxical membrane depolarization and Na+ overload, major and reversible contributors to weakness by ion channel leaks. Proceedings of the National Academy of Sciences of the United States of America 106:4036-4041.
10. Yang, B., Y. Yang, W. L. Tu, Y. Shen, and Q. Dong. 2014. A rare case of unilateral adrenal hyperplasia accompanied by hypokalaemic periodic paralysis caused by a novel dominant mutation in CACNA1S: features and prognosis after adrenalectomy. Bmc Urol 14.
11. Chabrier, S., N. Monnier, and J. Lunardi. 2008. Early onset of hypokalaemic periodic paralysis caused by a novel mutation of the CACNA1S gene. Journal of Medical Genetics 45:686-688.
12. Matthews, E., R. Labrum, M. G. Sweeney, R. Sud, A. Haworth, P. F. Chinnery, G. Meola, S. Schorge, D. M. Kullmann, M. B. Davis, and M. G. Hanna. 2009. Voltage sensor charge loss accounts for most cases of hypokalemic periodic paralysis. Neurology 72:1544-1547.
13. Hirano, M., Y. Kokunai, A. Nagai, Y. Nakamura, K. Saigoh, S. Kusunoki, and M. P. Takahashi. 2011. A novel mutation in the calcium channel gene in a family with hypokalemic periodic paralysis. J Neurol Sci 309:9-11.
14. Ptacek, L. J., R. Tawil, R. C. Griggs, A. G. Engel, R. B. Layzer, H. Kwiecinski, P. G. McManis, L. Santiago, M. Moore, G. Fouad, and et al. 1994. Dihydropyridine receptor mutations cause hypokalemic periodic paralysis. Cell 77:863-868.
15. Lehmann-Horn, F., I. Sipos, K. Jurkat-Rott, R. Heine, H. Brinkmeier, B. Fontaine, L. Kovacs, and W. Melzer. 1995. Altered calcium currents in human hypokalemic periodic paralysis myotubes expressing mutant L-type calcium channels. Soc Gen Physiol Ser 50:101-113.
16. Nishimoto, K., S. A. Tomlins, R. Kuick, A. K. Cani, T. J. Giordano, D. H. Hovelson, C.-J. Liu, A. R. Sanjanwala, M. A. Edwards, C. E. Gomez-Sanchez, K. Nanba, and W. E. Rainey. 2015. Aldosterone-stimulating somatic gene mutations are common in normal adrenal glands.

Proceedings of the National Academy of Sciences 112:E4591-E4599.
17. Azizan, E. A., H. Poulsen, P. Tuluc, J. Zhou, M. V. Clausen, A. Lieb, C. Maniero, S. Garg, E. G. Bochukova, W. Zhao, L. H. Shaikh, C. A. Brighton, A. E. Teo, A. P. Davenport, T. Dekkers, B. Tops, B. Kusters, J. Ceral, G. S. Yeo, S. G. Neogi, I. McFarlane, N. Rosenfeld, F. Marass, J. Hadfield, W. Margas, K. Chaggar, M. Solar, J. Deinum, A. C. Dolphin, I. S. Farooqi, J. Striessnig, P. Nissen, and M. J. Brown. 2013. Somatic mutations in ATP1A1 and CACNA1D underlie a common subtype of adrenal hypertension. Nat Genet 45:1055-1060.
18. Ophoff, R. A., G. M. Terwindt, M. N. Vergouwe, R. van Eijk, P. J. Oefner, S. M. Hoffman, J. E. Lamerdin, H. W. Mohrenweiser, D. E. Bulman, M. Ferrari, J. Haan, D. Lindhout, G. J. van Ommen, M. H. Hofker, M. D. Ferrari, and R. R. Frants. 1996. Familial hemiplegic migraine and episodic ataxia type-2 are caused by mutations in the Ca2+ channel gene CACNL1A4. Cell 87:543-552.
19. Kraus, R. L., M. J. Sinnegger, H. Glossmann, S. Hering, and J. Striessnig. 1998. Familial hemiplegic migraine mutations change alpha1A Ca2+ channel kinetics. J Biol Chem 273:5586-5590.
20. Hans, M., S. Luvisetto, M. E. Williams, M. Spagnolo, A. Urrutia, A. Tottene, P. F. Brust, E. C. Johnson, M. M. Harpold, K. A. Stauderman, and D. Pietrobon. 1999. Functional consequences of mutations in the human alpha1A calcium channel subunit linked to familial hemiplegic migraine. J Neurosci 19:1610-1619.
21. van den Maagdenberg, A. M., D. Pietrobon, T. Pizzorusso, S. Kaja, L. A. Broos, T. Cesetti, R. C. van de Ven, A. Tottene, J. van der Kaa, J. J. Plomp, R. R. Frants, and M. D. Ferrari. 2004. A Cacna1a knockin migraine mouse model with increased susceptibility to cortical spreading depression. Neuron 41:701-710.
22. Ducros, A., C. Denier, A. Joutel, M. Cecillon, C. Lescoat, K. Vahedi, F. Darcel, E. Vicaut, M. G. Bousser, and E. Tournier-Lasserve. 2001. The clinical spectrum of familial hemiplegic migraine associated with mutations in a neuronal calcium channel. N Engl J Med 345:17-24.
23. Battistini, S., S. Stenirri, M. Piatti, C. Gelfi, P. G. Righetti, R. Rocchi, F. Giannini, N. Battistini, G. C. Guazzi, M. Ferrari, and P. Carrera. 1999. A new CACNA1A gene mutation in acetazolamide-responsive familial hemiplegic migraine and ataxia. Neurology 53:38-43.
24. Kraus, R. L., M. J. Sinnegger, A. Koschak, H. Glossmann, S. Stenirri, P. Carrera, and J. Striessnig. 2000. Three new familial hemiplegic migraine mutants affect P/Q-type Ca(2+) channel kinetics. J Biol Chem 275:9239-9243.
25. Alonso, I., J. Barros, A. Tuna, A. Seixas, P. Coutinho, J. Sequeiros, and I. Silveira. 2004. A novel R1347Q mutation in the predicted voltage sensor segment of the P/Q-type calcium-channel alpha-subunit in a family with progressive cerebellar ataxia and hemiplegic migraine. Clin Genet 65:70-72.
26. Stam, A., K. Vanmolkot, H. Kremer, J. Gärtner, J. Brown, E. Leshinsky-Silver, R. Gilad, E. Kors, W. Frankhuizen, H. Ginjaar, J. Haan, R. Frants, M. Ferrari, A. Van Den Maagdenberg, and G. Terwindt. 2008. CACNA1A R1347Q: a frequent recurrent mutation in hemiplegic migraine. Clinical Genetics 74:481-485.
27. Miki, T., T. A. Zwingman, M. Wakamori, C. M. Lutz, S. A. Cook, D. A. Hosford, K. Herrup, C. F. Fletcher, Y. Mori, W. N. Frankel, and V. A. Letts. 2008. Two novel alleles of tottering with distinct Ca(v)2.1 calcium channel neuropathologies. Neuroscience 155:31-44.
28. Blumkin, L., M. Michelson, E. Leshinsky-Silver, S. Kivity, D. Lev, and T. Lerman-Sagie. 2010. Congenital Ataxia, Mental Retardation, and Dyskinesia Associated With a Novel CACNA1A Mutation. J Child Neurol 25:892-897.
29. Friend, K. L., D. Crimmins, T. G. Phan, C. M. Sue, A. Colley, V. S. C. Fung, J. G. L. Morris, G. R. Sutherland, and R. I. Richards. 1999. Detection of a novel missense mutation and second

recurrent mutation in the CACNA1A gene in individuals with EA-2 and FHM. Human Genetics 105:261-265.

30. Tonelli, A., M. G. D'Angelo, R. Salati, L. Villa, C. Germinasi, T. Frattini, G. Meola, A. C. Turconi, N. Bresolin, and M. T. Bassi. 2006. Early onset, non fluctuating spinocerebellar ataxia and a novel missense mutation in CACNA1A gene. J Neurol Sci 241:13-17.